Toward an Aqueous Solar Battery: Direct Electrochemical Storage of Solar Energy in Carbon Nitrides

*Filip Podjaski, Julia Kröger, and Bettina. V. Lotsch**

Graphitic carbon nitrides have emerged as an earth-abundant family of polymeric materials for solar energy conversion. Herein, a 2D cyanamide-functionalized polyheptazine imide (NCN-PHI) is reported, which for the first time enables the synergistic coupling of two key functions of energy conversion within one single material: light harvesting and electrical energy storage. Photo-electrochemical measurements in aqueous electrolytes reveal the underlying mechanism of this "solar battery" material: the charge storage in NCN-PHI is based on the photoreduction of the carbon nitride backbone and charge compensation is realized by adsorption of alkali metal ions within the NCN-PHI layers and at the solution interface. The photoreduced carbon nitride can thus be described as a battery anode operating as a pseudocapacitor, which can store light-induced charge in the form of long-lived, "trapped" electrons for hours. Importantly, the potential window of this process is not limited by the water reduction reaction due to the high intrinsic overpotential of carbon nitrides for hydrogen evolution, potentially enabling new applications for aqueous batteries. Thus, the feasibility of light-induced electrical energy storage and release on demand by a one-component light-charged battery anode is demonstrated, which provides a sustainable solution to overcome the intermittency of solar radiation.

In the quest to reduce global warming and our reliance on fossil fuels, renewable energy has become a key technology driver and a major socioeconomic growth factor.[1] To circumvent the fluctuation and storage issues renewables are facing, different solutions are at hand, all of which however suffer from certain disadvantages. Solar energy produced by photovoltaic devices is typically stored decentralized in batteries, requiring decoupling of energy conversion and storage, which is both a major loss and cost factor. At the same time, batteries suffer from low power densities that pose problems to the versatility of batteries, especially regarding their use in mobile applications. This can in part be overcome by electrochemical capacitors, which are promising alternatives for high power applications on short time scales; these devices however still suffer from low energy densities. In principle, fuels provide a natural solution to bridge the "storage gap" as they can store high amounts of energy per mass in chemical bonds. Consequently, research efforts are being put into the production of solar fuels such as hydrogen or methane by means of photocatalysis. However, their implementation shifts the energy supply problem to the requirement of a viable infrastructure based on those alternative energy carriers, which is currently nonexistent on a large scale.

One desirable solution would thus be the on-site storage of solar energy light where it is produced—i.e., in the light absorber—in the form of readily usable electrical energy rather than chemical bonds. This would require the seamless combination of the elementary steps of light harvesting, charge carrier separation, and their storage to retrieve them as electrical energy on demand, ideally in one single, earth-abundant material.

Here, we report on a material that is able to harvest, store, and release solar energy in the form of electrical energy. The material is a 2D cyanamide (NCN^-)-functionalized polyheptazine imide (NCN-PHI),[2,3] which upon light excitation and extraction of photogenerated holes accumulates electrons in the form of stable π-radicals. Notably, these radicals can be visually discerned by their blue color. We have previously shown that such "trapped" electrons can be collected in the dark after a time delay of several hours by addition of a cocatalyst, which produces hydrogen on demand.[3] It is thus possible to decouple the absorption of solar energy from the catalytic step in the dark, thus mimicking the separation of light and dark reactions in natural photosynthesis.

We now take this concept one step further and propose a solar battery half-cell, which enables the absorption of light, and the storage of photoinduced electrons and their release in the form of electrical energy in one single carbon nitride material.

F. Podjaski, J. Kröger
Max Planck Institute for Solid State Research
Heisenbergstraße 1, 70569 Stuttgart, Germany
F. Podjaski
Ecole Polytechnique Fédérale de Lausanne
Station 12, 1015 Lausanne, Switzerland
J. Kröger, Prof. B. V. Lotsch
Department of Chemistry
University of Munich (LMU)
Butenandtstraße 5-13, 81377 München, Germany
E-mail: b.lotsch@fkf.mpg.de
Prof. B. V. Lotsch
Nanosystems Initiative Munich (NIM)
Schellingstraße 4, 80799 München, Germany
Prof. B. V. Lotsch
Center for Nanoscience
Schellingstraße 4, 80799 München, Germany
The ORCID identification number(s) for the author(s) of this article can be found under https://doi.org/10.1002/adma.201705477.

DOI: 10.1002/adma.201705477

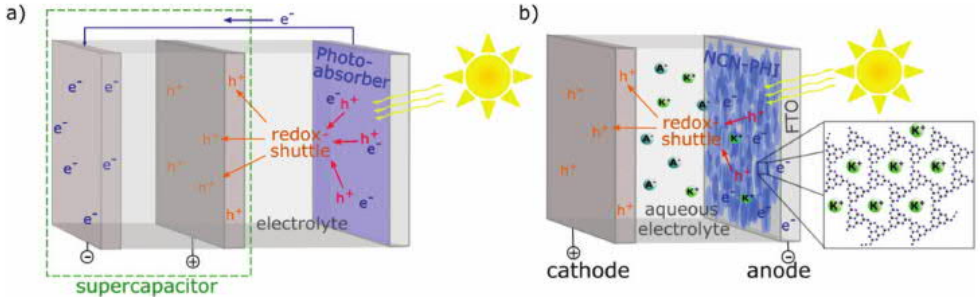

Figure 1. a) Concept of a traditional solar battery or solar photocapacitor. Photogenerated electrons and holes created in a photoabsorber are transported via an external circuit and a redox shuttle to an electrochemical storage device. The implementation shown here corresponds to that of a photo-supercapacitor. b) Proposed monolithic solar battery based on NCN-PHI. Photoabsorption and electron storage occurs within the same material. Holes are extracted to a counterelectrode via the electrolyte by a redox shuttle (or charge selective contact).

While the concept of a solar battery may be primarily associated with bulk electrodes, we emphasize the continuous transition from battery to pseudocapacitor materials with decreasing particle size and increasing surface area.[4] Our material solution provides several advantages over existing solar-powered electrochemical energy storage systems, the so-called "solar batteries."[5,6] These are integrated multicomponent solutions featuring different types of inorganic materials (**Figure 1**).[7] All approaches used to date are integrated devices based on photoelements that charge either supercapacitors or redox batteries.[5,8] This is also the case for other de facto "two-electrode" redox-based solar batteries where the photoabsorber forms a composite with one electrode by nanostructuring.[9] In our one-component system, the external charging circuit becomes redundant, thus reducing the complexity of the device significantly. The conceptual difference between the traditional solution and the realization of a photoabsorber with a charge storage ability proposed here is schematically shown in Figure 1a,b. Although photo-supercapacitors integrate a solar cell with a supercapacitor (Figure 1a), the photogenerated electrons need to be shuttled from the photoabsorber to the capacitor-type counterelectrode for storage through external wiring. In contrast, the proposed monolithic system is based on a photoanode that simultaneously absorbs light and locally stores photogenerated electrons in one single material (Figure 1b). The holes are extracted to a counterelectrode via some sort of redox shuttle in both cases.

In the following, we will concentrate on the dual light harvesting and charge storage/release functionality of NCN-PHI operating as the solar battery anode. Band gap irradiation (2.76 eV; see Figure S1.3 in the Supporting Information) of exfoliated NCN-PHI nanosheets deposited on fluorine doped tin oxide (FTO) substrate triggers the formation of electron–hole pairs, which subsequently have to be separated spatially.[2,3,10] This is usually achieved via a redox shuttle in a full solar battery, which however puts limitations to the overall cell kinetics. In order to mimic a cathode that swiftly takes up the holes, we therefore extract them chemically by a sacrificial electron donor, as previously described.[3,11] To this end, we add aqueous 4-methylbenzyl alcohol (4-MBA) as a reducing agent that acts both as a highly efficient and selective hole quencher,[11] thus allowing us to concentrate on the photoanode half-cell in the following.

In the first part, we evaluate key properties of the NCN-PHI solar battery anode—open-circuit potential (OCP), charge storage capacity, and the stability of the stored charges, i.e., the storage time. We then analyze the microscopic processes and limitations underlying the observed photo-electrochemical performance.

When the NCN-PHI photoelectrodes are illuminated with AM1.5 G solar radiation in O_2-free 1 M Na-based phosphate buffer solution (pH 7) in the presence of 4-MBA, the photocharge or OCP rises up to −800 mV vs Ag/AgCl (−600 mV vs NHE, +2.45 V vs Li) (see Figure 4a).[3] We can thus roughly distinguish between this charged, blue state and a ground or decayed state with an OCP around −200 mV vs Ag/AgCl. This photovoltage in the charged state represents the average potential of the highest energy levels occupied by the electrons, thus defining the half-cell voltage of this solar battery anode.

Next, we analyze the capacity of the photoanode by determining its charge storage properties. The resulting (solar) battery properties of our NCN-PHI photoelectrodes are summarized in **Figure 2.**

In order to estimate the maximum charge that can be extracted from the solar battery anode, we varied the discharge currents after 1 min of 1 sun illumination (AM1.5 G) in 1 M phosphate buffer and 5×10^{-3} M 4-MBA in order to find optimized charge extraction currents (see Figure 2a and Figure S2.1 in the Supporting Information). Current densities between 10 and 100 mA g^{-1} balance losses due to slow self-discharge at low currents (1 mA g^{-1}, red shaded) and high intrinsic resistive losses due to limited conductivity at high discharge currents (1 A g^{-1}, gray shaded). The optimum was found at 100 mA g^{-1} and was used for all further measurements.

To investigate the evolution of the stored charge and its stability, we increased the illumination time stepwise and measured the respective discharge curves shown in Figure 2b. Increasing illumination and thus charging times lead to an increase in charge storage up to 43.7 C g^{-1} (12.1 mA h g^{-1}) after 100 min of illumination. Longer illumination times above 12 h affect the electrode stability (as discussed in Sections S2.2 and S2.3 in the Supporting Information). Assuming an average mass of 231(2) g mol^{-1} per NCN-functionalized heptazine unit, 43.7 C g^{-1} correspond to one electron being stored on every 9th to 10th heptazine moiety. The average mass is obtained by assuming a cyanamide functionalization at every second heptazine, 0.58 potassium ions per functionalized heptazine units and deprotonated NH bridges, resulting in an overall neutral molecule (see Section S1 in the Supporting

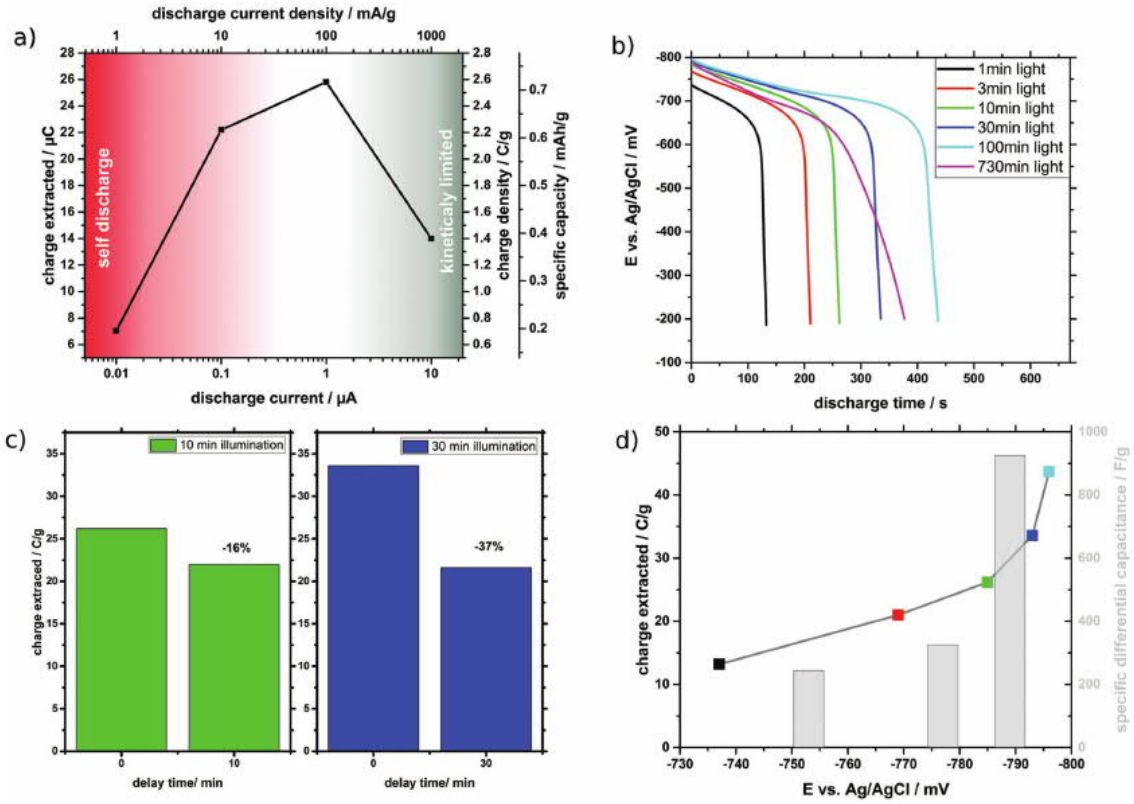

Figure 2. NCN-PHI solar battery half-cell characteristics summarizing the discharge properties of electrodes with 10 µg NCN-PHI, phosphate buffer, and 5×10^{-3} M 4-MBA. a) Evaluation of the total extracted charge after 1 min of illumination as a function of the discharge current densities varying from 1 mA g^{-1} to 1 A g^{-1} (raw data; Figure S2.1, Supporting Information). b) Discharge profiles at 100 mA g^{-1} showing increased charge storage after increasing illumination times. c) Comparison of the extracted charge after 10 min illumination and direct (0 min) or 10 min delayed discharge (left) as well as 30 min illumination and direct as well as 30 min delayed discharge (right). Raw data for delayed discharge, see Figure S2.2 in the Supporting Information. d) Extracted charge from (b) as a function of the corresponding electrode potential before the discharge and evaluation of the charge density (differential capacitance) resulting from the charge difference between the respectively attained voltage values.

Information). Note that the conjugation length of the imide-bridged polymer, which varies with the synthesis conditions, influences the amount of negative charge that can be trapped on the heptazine rings as well as its delocalization across the polymer backbone and, hence, its capacity profile. The fact that the extractable charge increases nonlinearly with illumination time (partly due to losses via the substrate as discussed further below; see Figure 4b and Section S2.2 in the Supporting Information) is beneficial to charge a solar battery continuously. This situation is in contrast to solar supercapacitors that attain their capacity limit within minutes and comparable to other solar batteries that are charged by a photoelement.[12]

To investigate for how long and efficiently this stored charge can be used after the illumination has stopped, we delayed the discharge after 10 and 30 min of illumination by 10 and 30 min, respectively, as shown in Figure 2c. Delaying the discharge by 10 min leads to a slightly decreased capacity of only 16%, while in the 30 min case, 37% are lost. This charge decay is related to Faradaic charge transfer from the partially uncovered FTO substrate to the electrolyte (see Section S2.2 in the Supporting Information).

The increased charge storage in the NCN-PHI correlates with the electrode potential, which becomes more negative with irradiation time, as shown in Figure 2d. The variable electrode potential and the amount of charge stored at each respective potential reflect the distribution of energy levels that are accessible to the photoinduced electrons, and is therefore an indirect measure of the electronic density of state (DOS), which formally translates into a differential capacitance. An analysis of the differential charge extracted after reaching the respective potentials thus allows us to estimate a differential capacitance ($C = Q/V$ or dQ/dV) in the respective potential windows. Note that due to the Faradaic losses the differential capacitance values we extract are likely underestimated. Increasing the illumination time from 10 to 30 min leads to a voltage difference of 8 mV (−785 to −793 mV vs Ag/AgCl) and a difference in extracted charge of 7.4 C g^{-1}. From this, a specific differential capacitance of 925 F g^{-1} can be extracted at an average intermediate potential of 789 mV, which is higher than, e.g., 379.9 F g^{-1} obtained from g-C3N4@graphene oxide at similar current densities of 250 mA g^{-1}.[13] Following the trend shown in Figure 2d, we expect even higher specific capacities if the photovoltage is increased even more, thus again highlighting the promise of NCN-PHI as a high-capacity solar battery photoanode. Note, however, that an evaluation of the differential capacitance after longer illumination times was hindered by electrode stability issues that could lead to an overestimation of the capacitance.

The long stability of the NCN-PHI discharge potential above –700 mV vs Ag/AgCl is due to the high DOS in this voltage region. Opposite to the fast voltage decay observed in common photocapacitors, which do not have a built-in storage option in the absorber and use separated capacitors,[8,14] this high DOS and capacitance in our material is a key property for a stable operation potential of a solar battery. For illumination times of only 1 min, the capacity of 13.2 C g^{-1} for our NCN-PHI photoanode is comparable to photocapacitors based on carbon nanotubes (CNT) with a capacitance of 17.5 C g^{-1}.[14] However, such CNT devices must be discharged within 2 min immediately after illumination due to fast self-discharge, a drawback that is circumvented by the long-term storage capacity of our material (see Figure S2.8 in the Supporting Information). As the potentials for electron storage are mostly more negative than –700 mV vs Ag/AgCl in phosphate buffer and even below –800 mV in KCl (corresponding to –100 and –200 mV vs RHE at pH7), the long-term stability of the charge storage on NCN-PHI is remarkable. Note that since NCN-PHI is unable to evolve hydrogen without the presence of a cocatalyst (see Section S2.2 in the Supporting Information: Decay via hydrogen evolution by NCN-PHI), this high overpotential for the hydrogen evolution reaction (HER) is thus a beneficial factor to increase the potential window of a solar battery anode operating in water.

An interesting aspect in terms of charge storage properties is the question whether NCN-PHI can also be charged purely electrically, i.e., by application of a negative bias and without the presence of a sacrificial donor in the dark. We therefore cycled NCN-PHI electrodes electrically in the dark in 1 M phosphate buffer to investigate the battery charging and discharging properties at 100 mA g^{-1} as shown in **Figure 3**. We find that reversible electrical charging and discharging is indeed possible. The charge required to reach a potential of –800 mV vs Ag/AgCl is slightly higher than the charge that can be extracted subsequently which is attributed to partial charge transfer to the electrolyte from uncovered substrate parts (see Section S2.2 in the Supporting Information). The specific charge extracted on the discharge (45–60 C g^{-1}, Figure 3b) is in good agreement with measurements after light charging up to almost –800 mV vs Ag/AgCl (see Figure 2d) although the electrical measurement underestimates the full capacity. While a complete charging of the electrode material is possible by sunlight in the presence of a donor, purely electrical charging is limited by slow kinetics and low conductivity of the NCN-PHI films, giving rise to a potential drop across the material. It therefore does not allow charging the electrode homogenously in a short period of time and thus underestimates the capacity of the whole material.

This point is further discussed later in the text. Figure 3a,b shows a decrease in capacity with increasing cycle number, which is attributed to a lack in mechanical stability of the sample (see discussion in Section S2.3 in the Supporting Information). To decouple the mechanical stability from the charge–discharge stability, we assume that the charge extracted at the discharge correlates with the mechanical stability (i.e., the leftover material), while the evolution of the ratio between charge stored and charge extracted (Coulombic efficiency) provides a good measure for the electronic charge–discharge stability. As visible in the inset of Figure 3b, the evolution of this Coulombic efficiency quickly approaches a constant value of 75%–80% with increasing cycle number, indicating continuously good electronic stability of the NCN-PHI nanosheets after some initial charging cycles that activate the material. This highlights that the lifetime limitations are most probably purely mechanical, i.e., limited by adhesion. The observed Coulombic efficiencies are even above the value of 45% observed in melon-type carbon nitride (dark) battery anodes.[15]

For a better understanding of the microscopic processes that both enable and limit solar and electrical energy storage in NCN-PHI, further photo-electrochemical experiments have been performed. First, we address the accessible OCP under different conditions. If the NCN-PHI electrodes are illuminated without a dedicated donor in pure water or phosphate buffer, an OCP of –170 and –570 mV vs Ag/AgCl, respectively, is observed, which is caused by the presence of some photoelectrons in the conduction band (see **Figure** 4a, pink and

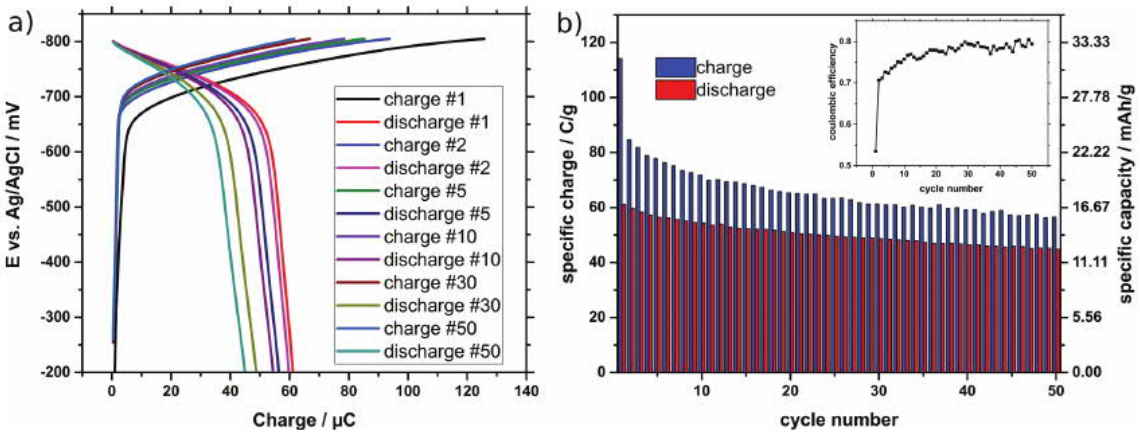

Figure 3. Cyclic electrical charging and discharging profiles (50 cycles) with 100 mA g^{-1} between –200 and –800 mV vs Ag/AgCl in phosphate buffer. a) Selected profiles of the 1st, 2nd, 5th, 10th, 30th, and 50th charging and discharging cycles. The relatively slow voltage increase above –700 mV vs Ag/AgCl underlines the increased capacitance in that region. b) Evolution of the charge stored and extracted during 50 cycles. While the overall charge stored and extracted decreases with increasing cycle number, the Coulombic efficiency (inset) approaches a constant value of ≈80%, indicating a good electronic stability.

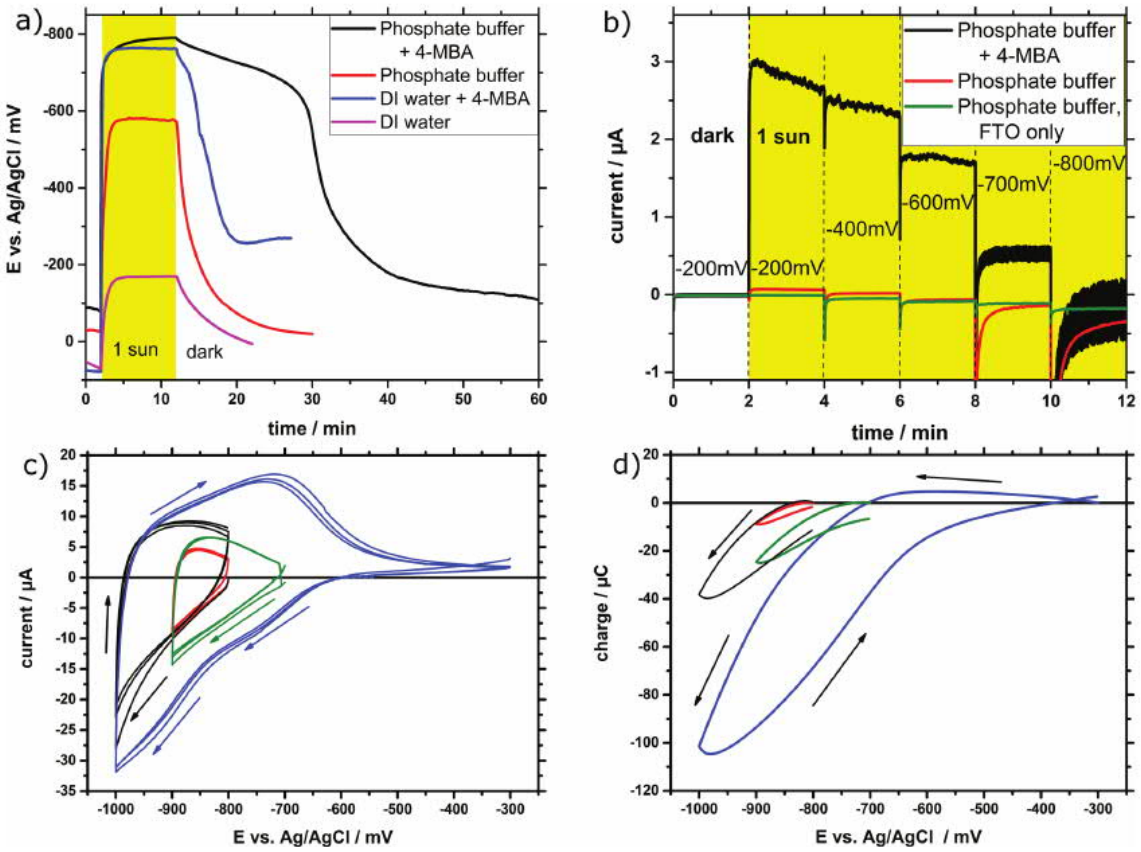

Figure 4. (Photo)electrochemical measurements on NCN-PHI electrodes. a) OCP measurements before, during, and after 10 min of 1 sun illumination, showing the potential and the stability of stored photoelectrons depending on the electrolyte and donor. b) (Dis)charging currents at different potentials under illumination in the presence of a donor and without, providing a measure of electron generation and self-discharge currents under illumination. c) *CV* scans at 50 mV s^{-1} in the dark in 1 M KCl for different potential windows, highlighting the voltage-dependent charge storage ability of NCN-PHI electrodes. d) Charge stored in and withdrawn from the electrode during the respective scans in (c).

red curves). These OCP values can thus be attributed to the electron quasi-Fermi-level under 1 sun illumination and is due to a balance between charge generation and recombination. The higher OCP in the phosphate buffer case is attributed to a small capacitive stabilization of the photoelectrons that will be discussed in more detail below. When the donor 4-MBA is added, the OCP value is again −800 mV vs Ag/AgCl, thus 200 mV more negative than in the case with only phosphate buffer (blue and black curves, respectively): since now the holes are quenched and electrons can accumulate, they reach more negative states. Furthermore, the charging process continues if both donor and phosphate buffer are present, which leads to a gradual increase in the OCP (see difference between black and blue curves) as well as a more stable electrode potential after illumination, i.e., a delayed decrease in potential after the light is switched off. This phenomenon points again to a capacitive storage of electrons in the potential window more negative than −600 mV vs Ag/AgCl, as discussed further below.

To investigate the amount of charges per second that are effectively generated and stored in NCN-PHI upon illumination, i.e., the electron generation currents, we measured the photocurrents at different potentials vs Ag/AgCl applied to the NCN-PHI@FTO electrodes in the presence and absence of a donor (see Figure 4b). A negative current corresponds to electron injection through the FTO substrate into the NCN-PHI or into the electrolyte, while a positive current is a measure for photoelectrons withdrawn from the material (i.e., the desired process). Without any illumination, an applied voltage of −200 mV vs Ag/AgCl corresponds to dark OCP conditions and no current flow is observed for all cases. Under illumination and in the presence of a donor, the application of a bias of +600 mV (i.e., a working potential at −200 mV vs Ag/AgCl) creates an extraction driving force with respect to the electrons being present in the conduction band (CB) and leads immediately to a positive charge extraction current. It is an order of magnitude higher than without 4-MBA (Figure 4b, black curve vs red/green curves). This highlights the importance of an efficient hole extraction to charge the electrode efficiently and to stabilize the charges in low voltage states. With an increasing negative voltage that is applied as indicated in Figure 4b, the driving force for hole extraction decreases and so does the current until the applied voltage is −800 mV vs Ag/AgCl (see black curve). The small positive current, even without a dedicated donor (red curve), highlights that a kinetically hindered oxidation of the phosphate buffer or water is possible, which is consistent with the valence band lying well below the required potentials for these reactions.[11,16] In other words, water can

also act as a donor for NCN-PHI, but is less efficient than 4-MBA.

Without donor, we already observe a negative current at −600 mV vs Ag/AgCl, arising from electron injection into the conduction band of the material as the applied potential is more negative than the OCP under illumination. In the same voltage region (< −600 mV), the FTO substrate shows a small negative current due to redox reactions with the electrolyte (water reduction or phosphate reduction).[17] From this we can deduce that the charging currents for NCN-PHI electrodes in this potential range are limited by self-discharge involving electrons being injected back through the substrate into the electrolyte. Although this process is orders of magnitude smaller compared to the charging currents with a donor present, it nevertheless presents a loss channel explaining the discrepancy between the direct and delayed discharging processes shown in Figure 2c (see discussion in Section S2.2 in the Supporting Information). Hence, a complete coverage of the substrate with NCN-PHI is crucial to achieve a stable OCP after illumination, which remains to be optimized.

To further study the role of ions for the energy storage process and its kinetics, we cycled the electrodes electrochemically in the dark. Figure 4c shows the current–voltage (*CV*) measurements of NCN-PHI@FTO electrodes in 1 M KCl in different potential windows. KCl was chosen instead of phosphate buffer due to the better electrochemical stability of the electrolyte (no reaction with phosphates possible) and the improved cycling stability of the electrodes (Figures S2.5 and S2.6, Supporting Information; similar data for measurements in phosphate buffer are shown and discussed in Figure S2.13 in the Supporting Information). The blue curve (−300 to −1000 mV vs Ag/AgCl) shows that a significant current flows into the electrode starting from −600 mV vs Ag/AgCl, first with a flatter slope, then with an increasing slope from −800 mV onward. The shape of the curves suggests that (i) the charge transfer is capacitive in nature and (ii) the charge uptake by the NCN-PHI electrode, and, hence, also the charge extracted from NCN-PHI, is dependent on the absolute potential window. This further proves different capacitive regimes for electron uptake, corresponding to a potential-dependent DOS in the conduction band that is increasing with negative potential, in agreement with Figure 2d. The presence of kinetic limitations of this charge storage and release process are best visible in the blue scan in Figure 4c,d and in the data shown in Figure S2.13 (Supporting Information). It requires a whole scan back to −300 mV and forward to −600 mV to release all the charges stored in the conduction band below −600 mV vs Ag/AgCl before a refilling of the NCN-PHI at more negative potentials starts again (Figure 4c,d, blue curve vs other curves). This behavior puts a limit to the discharge kinetics, indicating that a fast discharge is not able to extract all the electrons in the CB, as previously observed in Figure 2a and the galvanostatic charge and discharge experiments in Figure 3. Possible causes for this effect are an increase in electronic conductivity if the CB is gradually filled, similar to TiO_2,[18] which is discussed in the following text, or a kinetically limited pseudocapacitance that enhances charge transport and stabilizes the negative charge on the material by the in-diffusion and adsorption of alkali metal ions, i.e., a diffusion-limited mass transport process, or both. In fact, scan-rate-dependent measurements in the region between −700 and −900 mV vs Ag/AgCl (see Figures S2.9–S2.11 in the Supporting Information) show linearly increasing positive peak currents that follow pseudocapacitive behavior rather than a double-layer capacitance that should follow a square root dependency.[19] This is an indirect proof of the stabilization of the negative charge (i.e., "trapped electrons") by alkali metal ion adsorption. This screening of the negative charge is also the reason for the observed increased OCP without donor in the case of phosphate buffer vs pure water (Figure 4a, red vs pink curve). Control *CV* experiments without alkali metal ions present in the solution have been performed with 1 M tetrabutylammonium chloride (TBA-Cl) and did not show any positive currents (Figure S2.12 in the Supporting Information and other control experiments in Figures S2.9–S2.11(Supporting Information)), indicating that TBA cations are unable to support charge storage in this material. This clearly highlights the importance of an appropriate cation size (or more specifically, its hydrodynamic or equivalent Stokes radius) in order to penetrate the structural pores of NCN-PHI (3.8(4) Å) and thus to stabilize the electron storage by a pseudocapacitive process.[20] Solvated TBA ions (4.95 Å) seem to be too large to penetrate the pores, while Na^+ (1.84 Å) and K^+ (1.25 Å) both fit inside the pores, thus enabling pseudocapacitive charge stabilization.[21]

To further investigate the influence of illumination on the role of the counter ions as well as the mobility of charge carriers in NCN-PHI electrodes, we performed impedance measurements in the ground state voltage region (−24 mV vs Ag/AgCl) and in the charged or "activated" region (−850 mV vs Ag/AgCl), in KCl, again due to a more pronounced capacitive response, see **Figure 5**a,b. The data are fitted by an equivalent circuit diagram, which can be deduced from generalized equivalent circuits,[22] see the inset in Figure 5a. It accounts for series resistance losses in both, the electrode contact and the electrolyte, and includes a constant phase element accounting for double-layer capacitance Q_{DL} in parallel to a charge transfer resistance as well as a constant phase element accounting for pseudocapacitance Q_P in parallel to a resistive element R_C, accounting for the materials' conductivity. The measurement under illumination (blue curve) shows a significantly lower charge transfer resistance (i.e., better conductivity) with respect to the one measured in the dark (black curve). The appearance of an additional semicircle at higher frequencies is due to changes in the respective capacitive and conductive parameters (see Table S2.14 in the Supporting Information and discussion). The dominant contribution to the capacitance shifts from double-layer capacitance (5.9 F g^{-1}, black curve, dark measurement) to pseudocapacitance (blue curve, illuminated) and becomes as high as 191 F g^{-1}. The increasing value with respect to *CV* measurements beforehand (Figures S2.9–S2.11, Supporting Information) is due to more homogeneous charging as discussed above and in the graph, and is approaching the differential capacitance values extracted from the measurements under illumination in Figure 2d.

The apparent increase in conductivity that is observed in the blue state can be due to either increased electronic or ionic conductivity in the (light) charged state in an aqueous environment. To distinguish between both effects, the purely light-dependent conductivity was determined by sandwiching NCN-PHI between

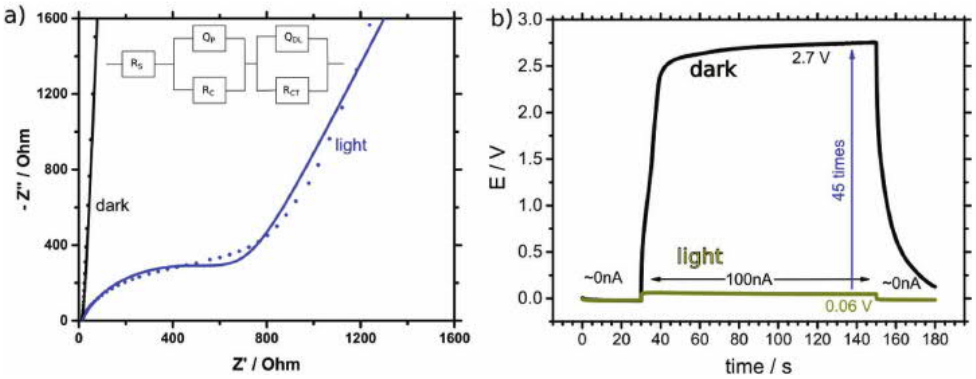

Figure 5. Conductivity of NCN-PHI nanosheets on FTO. a) Impedance measurements in oxygen-free 1 M KCl + 5 × 10^{-3} M 4-MBA in the yellow ground state (black curve: measurement and fit) and in the light induced, blue state (blue curve) which shows a significantly lower charge transfer resistance. Insets: Equivalent circuit diagram used to fit the data. b) Galvanostatic two-point resistivity measurements on an FTO–NCN-PHI–FTO electrode sandwich measured in air. The voltage drop due to resistance in the dark is 45 times higher than in the illuminated case (beige).

two FTO electrodes and measuring their DC conductivity galvanostatically in air. Since FTO is conductive only for electrons and blocking to ions, the measured equilibrium potential corresponds to the electronic conductivity of NCN-PHI alone. The measurement results are shown in Figure 5b. After an equilibration period of 30 s at 0 nA, a current of 100 nA has been forced through the sandwich for 120 s. Afterwards, the current was set back to 0 nA. During the whole process, the voltage drop over the sample was recorded. Comparing the measurement in complete darkness to the one where the sample was illuminated (≈7 sun) during the 120 s period of current flow, a resistance reduction of NCN-PHI by a factor of 45 is observed (27 MΩ in the dark compared to 600 kΩ under illumination). This indicates that light-induced electrons in the conduction band—even without the presence of a hole quencher—enhance the conductivity of the material significantly. It furthermore rationalizes why NCN-PHI photoelectrodes can be used more efficiently when charged by light rather than purely electronically, which is due to a decrease in resistive losses as further discussed in Section S4 in the Supporting Information. While locally increased photoconductivity in melon-type carbon nitrides has been observed several times by means of impedance measurements and photocurrents,[23] this represents the first direct evidence for enhanced long-range DC conductivity in carbon nitrides under illumination, to the best of our knowledge.

Taken the above evidence together, the mechanism of the observed light-induced pseudocapacitive behavior of NCN-PHI can be traced back to the following microscopic origin:

(i) The unique ability of NCN-PHI—in contrast to other carbon nitrides—to "store" electrons upon photoreduction, likely assisted by the electron-poor character and 2D conjugation of the imide-bridged heptazine backbone, as well as an extremely efficient hole extraction by the sacrificial electron donor. The latter aspect is general and works for a range of sacrificial electron donors,[3] which ultimately should simplify the hole transfer to a cathode in the presence of an appropriate hole shuttle in an overall solar battery configuration.

(ii) Screening of the light-induced electrons by alkali ions via diffusion into and through the structural pores of NCN-PHI as well as the mobile alkali ions that are provided and replenished through the electrolyte (see **Figure 6**). This interaction between the electrons that accumulate on the heptazine backbone and the cations that rearrange in the pores and in solution seems to be vital for high capacity and long-term electron storage, but at the same time limits the kinetics of the charge storage and release.

(iii) Light-induced increase in electronic conductivity of NCN-PHI. This feature is diagnostic of improved charge transport through the electrode under solar irradiation, which is likely due to the increased density of states accessible to the photoinduced electrons, see also Figure 6. An implication of this observation is that NCN-PHI shows improved charge storage and release when operated by light rather than when charged purely electrically.

The interplay between these processes is schematically summarized in Figure 6. The charge storage performance of the NCN-PHI electrode is currently limited by nonoptimized adhesion to the substrate for drop cast electrodes and the slow self-discharge processes occurring via the FTO substrate (e.g., reduction of the electrolyte), becoming significant at long delay times between light-induced charge storage and subsequent electrical extraction (see Figure 2b,c). Following the trend in Figure 2d, we expect even higher specific capacities if the photovoltage can be further increased, which would be equivalent on the microscopic level to a higher electron storage density than one in every 9th heptazine unit. In fact, if every heptazine unit would store one electron, a capacity of more than 100 mA h g^{-1} could be achieved and NCN-PHI would be compatible to actual carbon based supercapacitors operating only in the dark.[24] On the other hand, a more negative anode voltage, going hand in hand with such an increased charge storage, is contingent on decreasing the parasitic currents. Such loss channels can be reduced for example by optimizing the surface coverage of NCN-PHI and/or the choice of substrate, such that even higher OCPs are clearly realistic.

A noticeable feature of our solar battery half-cell is the fact that the electron storage occurs at very negative potentials, up to −850 mV vs Ag/AgCl (−240 mV vs RHE at pH7), enabling a large potential window when operated in water. Since the energy stored scales linearly with the capacitance *C*

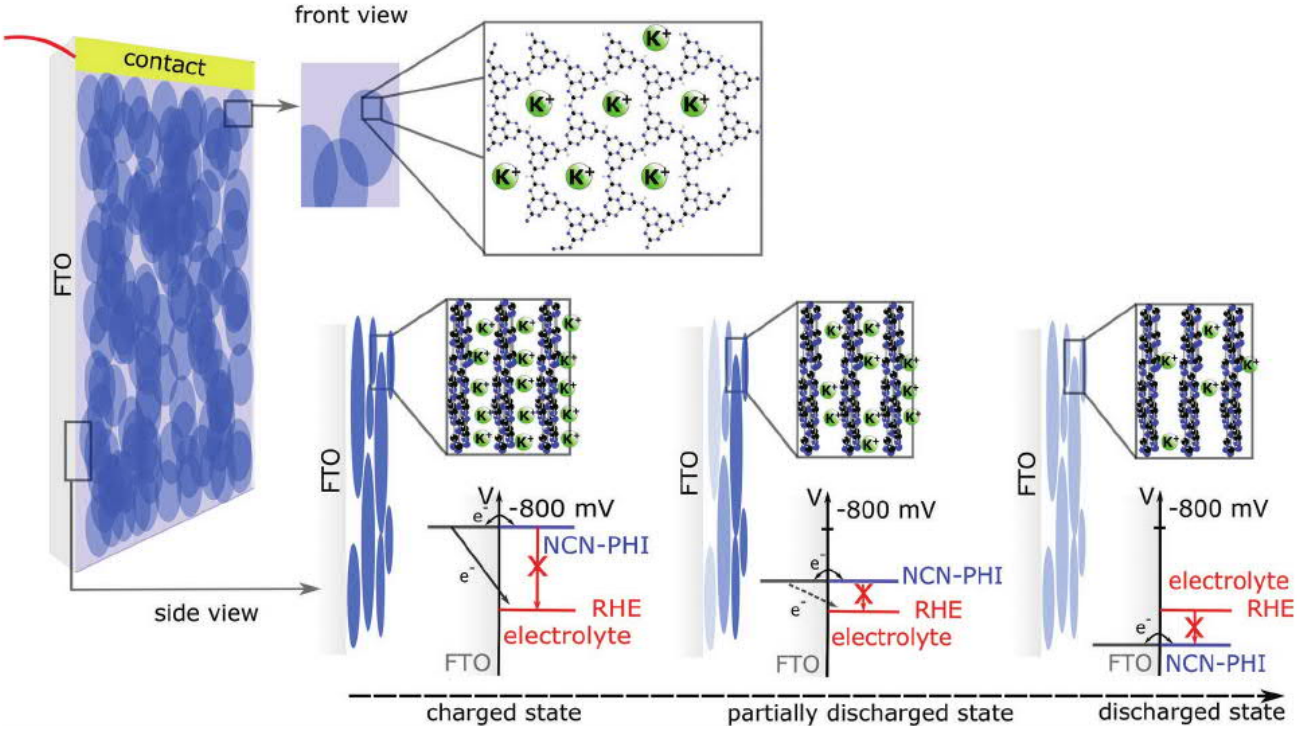

Figure 6. Schematics of a layered NCN-PHI photoelectrode, illustrating the role of alkali metal cations from the solution that can access the pores and stabilize the electronic charge on the NCN-PHI by pseudocapacitance. Note that the effectiveness of charge stabilization is thus a diffusion-limited process that is significantly influenced by the structure (pore size and alignment) and morphology (surface area) of the carbon nitride. Since discharging starts from the inner parts of the NCN-PHI film which are in close contact to the substrate (shown in light blue color), the morphology-limited percolation of charge carriers affects the material's conductivity at high current densities. The evolution from a charged to a discharged state is illustrated in the bottom part, showing the potential measured at the FTO surface, possible charge transfer paths between FTO, NCN-PHI and the electrolyte, as well as the role of alkali metal ions from the electrolyte that enables pseudocapacitive screening of the trapped electrons.

and quadratically with the potential difference V between the anode and the cathode via $E = 1/2\ CV^2$, the high overpotential of NCN-PHI for HER (Section S2.2, Supporting Information) pushes the fundamental limits of the energy that can be stored in aqueous batteries without parasitic water reduction occurring.

The amount of energy that could be extracted from a full battery depends on the energy levels of both the stored electrons and holes. With the conduction band lying approximately at –800 mV vs Ag/AgCl,[3] the material's large band gap of 2.76 eV allows for a reasonable tradeoff between visible light absorption and a high cell voltage.[25] For an estimation of the potential of a full battery we assume a system comparable to the one published by Wu and co-workers where an aqueous Li–I electrolyte is used in a solar flow battery with a Pt electrode as cathode.[26] The valence band holes (+1.9 V vs Ag/AgCl) would be stored in the electrolyte using the I^-/I_3^- redox couple at +330 mV vs Ag/AgCl.[27] The overall potential of a full battery would thus be around 1.13 V. Combining this potential with the capacity of 43.7 C g^{-1} (12.1 mA h g^{-1}) (Figure 2), a corresponding energy density of 49.4 J g^{-1} (13.7 Wh kg^{-1}) and a power density of 0.11 kW kg^{-1} (assuming the anode to be rate limiting) at discharge currents of 100 mA g^{-1} as used in Figure 2 with a discharge rate corresponding to 8.6 C would be realistic. Note that this is a very conservative estimate since the valence band of NCN-PHI is very positive, thus allowing for redox shuttles and cathodes with far more positive potentials. In addition, the oxygen evolution reaction, which would be a limiting reaction in an aqueous environment, has higher overpotentials than the hydrogen evolution reaction, thus likely allowing for even higher cell voltages.

In summary, we have shown that NCN-PHI, an earth-abundant and cheap material with an easy and scalable synthesis from organic precursors, can be used as a solar battery anode by the combination of two key optoelectronic properties—light absorption and electrical energy storage—within the very same material. To the best of our knowledge, this is the first example of such a dual functionality that is essential to reduce the complexity and applicability of solar batteries or solar-powered electrochemical energy storage systems. At the same time, this material allows for on-site or decentralized storage of renewable energies in the form of electricity and, hence, to bypass solar fuel production. The capacity and stability of charge storage is contingent on the pseudocapacitive incorporation of alkali metal ions into the porous 2D-NCN-PHI network. Since the material has a high intrinsic overpotential for water reduction, it shows an increased potential window for operating in an aqueous environment, thus promising significantly higher energy densities than in existing aqueous batteries. The capacity of NCN-PHI has been shown to be potential dependent and its conductivity is increased by illumination. Nevertheless, the low conductivity of NCN-PHI in its uncharged state limits its applicability to thin films with high power densities or thick films with higher charge retention abilities (i.e., higher

energy density if used as battery anode), at the expense of power density. Therefore, morphology engineering will be key to overcome charge percolation issues in this system. Finally, in order to create a full aqueous solar battery, a technically convenient solution for hole transport to a battery cathode remains to be found.

While we have focused here on the potential of NCN-PHI as a solar battery anode, the light-induced charge storage capability and conductivity enhancement observed in NCN-PHI are intriguing features for a number of other light-driven devices, ranging from organic-based electrochromic materials to photodriven resistive switches and photodetectors. Studies along these lines are ongoing in our lab. Taken together, the findings reported herein may present a key step toward an economy based not only on renewable energy, but also on renewable materials to build and power its infrastructure.

Supporting Information

Supporting Information is available from the Wiley Online Library or from the author.

Acknowledgements

This work was supported by an ERC Starting Grant (B.V.L., Grant No. 639233), the Max Planck Society, the Max Planck-EPFL Center for Molecular Nanoscience and Technology, the cluster of excellence Nanosystems Initiative Munich (NIM), and the Center for Nanoscience (CeNS). The authors are grateful to Dr. Rotraut Merkle for insightful discussions and her assistance with the data evaluation. The authors would like to thank Viola Duppel for TEM and SEM images, Marie-Claire Pignié and Philipp-Conrad Imhof for assistance in electrode preparation, as well as Dr. Vincent W.-h. Lau and Hendrik Schlomberg for fruitful discussions.

Conflict of Interest

The authors declare no conflict of interest.

Keywords

carbon nitrides, pseudocapacitance, solar batteries, solar energy conversion

Received: September 21, 2017
Revised: November 7, 2017
Published online: January 10, 2018

[1] a) N. S. Lewis, D. G. Nocera, *Proc. Natl. Acad. Sci. USA* **2006**, *103*, 15729; b) M. Z. Jacobson, *Energy Environ. Sci.* **2009**, *2*, 148; c) M. Z. Jacobson, M. A. Delucchi, *Sci. Am.* **2009**, *301*, 58; d) M. Z. Jacobson, M. A. Delucchi, *Energy Policy* **2011**, *39*, 1154; e) M. A. Delucchi, M. Z. Jacobson, *Energy Policy* **2011**, *39*, 1170.

[2] V. W. H. Lau, I. Moudrakovski, T. Botari, S. Weinberger, M. B. Mesch, V. Duppel, J. Senker, V. Blum, B. V. Lotsch, *Nat. Commun.* **2016**, *7*, 12165.

[3] V. W. Lau, D. Klose, H. Kasap, F. Podjaski, M. C. Pignie, E. Reisner, G. Jeschke, B. V. Lotsch, *Angew. Chem. Int. Ed. Engl.* **2017**, *56*, 510.

[4] a) P. Balaya, A. J. Bhattacharyya, J. Jamnik, Yu. F. Zhukovskii, E. A. Kotomin, J. Maier, *J. Power Sources* **2006**, *159*, 171; b) J. Maier, *Chem. Mater.* **2014**, *26*, 348; c) B. E. Conway, *J. Electrochem. Soc.* **1991**, *138*, 1539.

[5] M. Z. Yu, W. D. McCulloch, Z. J. Huang, B. B. Trang, J. Lu, K. Amine, Y. Y. Wu, *J. Mat. Chem. A* **2016**, *4*, 2766.

[6] H. G. Wei, D. P. Cui, J. H. Ma, L. I. Chu, X. O. Zhao, H. X. Song, H. Liu, T. Liu, N. Wang, Z. Guo, *J. Mat. Chem. A* **2017**, *5*, 1873.

[7] a) A. Takshi, T. Tevi, F. Rahimi, in *Next Generation Technologies for Solar Energy Conversion VI*, Vol. *9562*, (Eds: O. V. Sulima, G. Conibeer), SPIE, San diego **2015**, http://dx.doi.org/10.1117/12.2187671; b) Y. Sun, X. Yan, *Solar RRL* **2017**, *1*, 1700002.

[8] C. H. Ng, H. N. Lim, S. Hayase, I. Harrison, A. Pandikumar, N. M. Huang, *J. Power Sources* **2015**, *296*, 169.

[9] A. Hauch, A. Georg, U. O. Krasovec, B. Orel, *J. Electrochem. Soc.* **2002**, *149*, A1208.

[10] H. Xu, J. Yan, X. J. She, L. Xu, J. X. Xia, Y. G. Xu, Y. H. Song, L. Y. Huang, H. M. Li, *Nanoscale* **2014**, *6*, 1406.

[11] H. Kasap, C. A. Caputo, B. C. M. Martindale, R. Godin, V. W. H. Lau, B. V. Lotsch, J. R. Durrant, E. Reisner, *J. Am. Chem. Soc.* **2016**, *138*, 9183.

[12] J. T. Xu, Y. H. Chen, L. M. Dai, *Nat. Commun.* **2015**, *6*, 8103.

[13] Y. B. Ding, Y. H. Tang, L. M. Yang, Y. X. Zeng, J. L. Yuan, T. Liu, S. Q. Zhang, C. B. Liu, S. L. Luo, *J. Mater. Chem. A* **2016**, *4*, 14307.

[14] G. Wee, T. Salim, Y. M. Lam, S. G. Mhaisalkar, M. Srinivasan, *Energy Environ. Sci.* **2011**, *4*, 413.

[15] Y. T. Gong, M. M. Li, Y. Wang, *ChemSusChem* **2015**, *8*, 931.

[16] X. C. Wang, K. Maeda, A. Thomas, K. Takanabe, G. Xin, J. M. Carlsson, K. Domen, M. Antonietti, *Nat. Mater.* **2009**, *8*, 76.

[17] W. M. Haynes, *CRC Handbook of Chemistry and Physics*, CRC Press, Florida **2014**.

[18] a) A. C. Fisher, L. M. Peter, E. A. Ponomarev, A. B. Walker, K. G. U. Wijayantha, *J. Phys. Chem. B* **2000**, *104*, 949; b) F. Fabregat-Santiago, G. Garcia-Belmonte, J. Bisquert, A. Zaban, P. Salvador, *J. Phys. Chem. B* **2002**, *106*, 334.

[19] a) V. Augustyn, J. Come, M. A. Lowe, J. W. Kim, P. L. Taberna, S. H. Tolbert, H. D. Abruna, P. Simon, B. Dunn, *Nat. Mater.* **2013**, *12*, 518; b) H. Angerstein-Kozlowska, J. Klinger, B. E. Conway, *J. Electroanal. Chem.* **1977**, *75*, 45.

[20] a) C. Largeot, C. Portet, J. Chmiola, P. L. Taberna, Y. Gogotsi, P. Simon, *J. Am. Chem. Soc.* **2008**, *130*, 2730; b) G. H. Lane, E. Jezek, *Electrochim. Acta* **2014**, *150*, 173.

[21] a) P. C. F. Pau, J. O. Berg, W. G. McMillan, *J. Phys. Chem.* **1990**, *94*, 2671; b) S. Sugiharto, T. M. Lewis, A. J. Moorhouse, P. R. Schofield, P. H. Barry, *Biophys. J.* **2008**, *95*, 4698.

[22] J. Jamnik, J. Maier, *Phys. Chem. Chem. Phys.* **2001**, *3*, 1668.

[23] a) R. K. Gupta, A. A. Al-Ghamdi, F. El-Tantawy, W. A. Farooq, F. Yakuphanoglu, *Mater. Lett.* **2014**, *134*, 149; b) J. H. Wang, C. Zhang, Y. F. Shen, Z. X. Zhou, J. C. Yu, Y. Li, W. Wei, S. Q. Liu, Y. J. Zhang, *J. Mater. Chem. A* **2015**, *3*, 5126; c) A. K. Diaz-Garcia, M. I. Diez-Garcia, T. Lana-Villarreal, R. Gomez, *Electrochim. Acta* **2016**, *219*, 453.

[24] B. Li, F. Dai, Q. F. Xiao, L. Yang, J. M. Shen, C. M. Zhang, M. Cai, *Energy Environ. Sci.* **2016**, *9*, 102.

[25] Y. Liu, N. Li, S. C. Wu, K. M. Liao, K. Zhu, J. Yi, H. S. Zhou, *Energy Environ. Sci.* **2015**, *8*, 2664.

[26] M. Z. Yu, W. D. McCulloch, D. R. Beauchamp, Z. J. Huang, X. D. Ren, Y. Y. Wu, *J. Am. Chem. Soc.* **2015**, *137*, 8332.

[27] P. Atkins, *Physical Chemistry*, 6th ed., W.H. Freeman and Company, New York **1997**.

